Vertical-cavity surface-emitting resonances in photonic crystal films

J. M. Pottage, E. Silvestre,* and P. St. J. Russell[†]

Optoelectronics Group, Department of Physics, University of Bath, Claverton Down, Bath BA2 7AY, United Kingdom

It is shown that thin films of dielectric, etched through with a suitably chosen lattice of holes, can support surface-emitting vertical resonances with very-high-cavity Q factors ($\sim 10^5$ in the case of Al_xGaAs_{1-x} on oxidized Al_yGaAs_{1-y}).   A Bloch-wave expansion is used to develop a complete vector-field analysis of these resonances and to reveal their underlying physics.   Since they do not require multilayer mirrors, such resonators are a practical and simple replacement for conventional vertical-cavity surface-emitting laser structures.   Other applications include wavelength-division-multiplexing components and highly sensitive gas detectors.   © 2001 Optical Society of America

OCIS codes: 310.6860, 230.3990, 230.5750, 250.7260, 230.3120.

1. INTRODUCTION

Photonic crystal films are currently being developed, for example, as in-plane laser microcavities[1] and miniature wavelength-division multiplexers.[2]   They have previously been used to form subminiature optical components.[3,4]   In this paper we analyze the surface-emitting resonances supported by such films and show that a lattice of air holes creates a highly effective vertical cavity without the need for multilayer mirrors above and below the layer.   This means that vertical cavities can be simply realized by periodic patterning in the plane, permitting simple production of large arrays of surface-emitting microlasers, each emission wavelength being determined by the local hole size and spacing.

A dielectric material, perforated with a lattice of parallel holes on the length scale of the wavelength of light, supports natural modes in the form of photonic Bloch waves.   These waves can be viewed as stable superpositions of many plane waves, the resulting interference patterns matching the periodicity of the lattice.[5]   The structure that we analyze here consists of a thin layer of such a material, the upper and lower interfaces being perpendicular to the axes of the holes (Fig. 1).

Bloch-wave optics is very different from conventional plane-wave optics.   For example, under the right conditions, a Bloch-wave ray (which points in the direction of its group velocity) can be totally internally reflected by a dielectric interface at any angle of incidence, including the case of normal incidence.   This makes it possible, by appropriate positioning of the critical angle, to design a layer in which the Bloch-wave reflection coefficient at normal incidence is arbitrarily close to 100%.   This suggests the use of photonic crystal films as high-Q-factor resonators.   To win a proper understanding of such resonances, we must disentangle the contributions to the fields of the various Bloch waves.   Otherwise, the photonic crystal film becomes a black box whose output is a complicated and inexplicable function of its input.

In this paper we use a mathematically rigorous and physically intuitive method to model the vertical-cavity surface-emitting resonances (VCSER's) of a photonic crystal film.   The method, based on a rigorous consideration of the Bloch waves in the film, was first proposed in 1995[5] and has been used to calculate the nonradiative guided modes that such films can also support.[6,7]   Low-finesse resonances were observed and analyzed in Ref. 8.   A full description of the positions and properties of the VCSER's is calculated in a few cases, and the results are explained with a simple toy model.

2. MATHEMATICAL METHOD

A brief outline of our calculation strategy is as follows. We first compute the Bloch waves of an infinitely thick photonic crystal film.   The in-plane magnetic-field components of these waves are obtained by solving the equation

$$\left[\nabla_p^2 + k^2\epsilon + \frac{1}{\epsilon}\nabla_p\epsilon \times \nabla_p \times \right] \mathbf{H}_p = \beta^2 \mathbf{H}_p, \quad (1)$$

where β is the propagation constant along the z axis (normal to the layer) of a particular Bloch mode, $\epsilon(x, y)$ is the dielectric constant of the film, and k is the vacuum wave vector.   The subscript p denotes that only the x and the y components are included in the operators and the vectors. The solutions of Eq. (1) constitute a complete basis in terms of which the field distribution inside a photonic crystal film can be expressed in the complex exponential Bloch-wave form:

$$\sum_i U_\nu^i \exp(j\mathbf{G}^i \cdot \mathbf{r}_p)\exp[j(\mathbf{k}_p \cdot \mathbf{r}_p \pm \beta z - kct)]. \quad (2)$$

Equation (1) can be reformulated as a Fourier-space matrix eigensystem

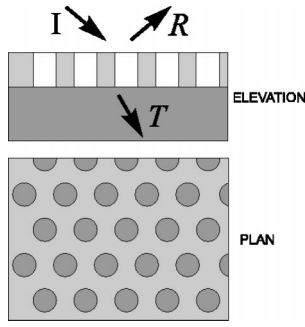$$\sum_{i,\mu} M_{\nu\mu}^{ji} U_\mu^i = \beta^2 U_\nu^j, \quad (3)$$

Fig. 1.   Schematic of the structure analyzed.   The holes penetrate the high-refractive-index film completely, stopping at the interface with the low-index substrate.   The holes are filled with air and the cover is air.

where the indices μ and ν stand for either of the in-plane coordinate axes x and y.   To calculate the elements of matrix $\mathbf{M}$, we use separate numerical Fourier expansions for the functions ϵ and $\epsilon^{-1}\nabla_p\epsilon$.   We avoid problems with convergence by modeling the lattice of holes as a triangular array of delta functions convolved with a super-Gaussian function:

$$\epsilon(r) = \epsilon_b + (\epsilon_a - \epsilon_b)\exp[-(r/w)^{2n}], \qquad (4)$$

where r is the radial position, w is the hole radius, and n is a positive integer.   This super-Gaussian function has the advantage that its Fourier expansion is uniformly convergent, unlike that of a step function.   Also, the super-Gaussian form is perhaps a closer fit to realistic fabricated structures.   We typically take $n = 3$.

To calculate how light interacts with the photonic crystal film, we need to impose boundary conditions on the fields at its upper and lower interfaces.   The in-plane components of the $\mathbf{E}$ and $\mathbf{H}$ fields must be continuous functions of position even where the refractive index has a finite discontinuity.   In the cover (cov) we have the following contributions to the total in-plane magnetic-field components:

$$\mathbf{H}_p^{\text{inc}} = \sum_i \mathbf{h}_{\text{inc}}^i \exp[j(\mathbf{G}^i + \mathbf{k}_p) \cdot \mathbf{r}_p - j\alpha_{\text{cov}}^i z - jkct],$$

$$\mathbf{H}_p^{\text{ref}} = \sum_i \mathbf{h}_{\text{ref}}^i \exp[j(\mathbf{G}^i + \mathbf{k}_p) \cdot \mathbf{r}_p + j\alpha_{\text{cov}}^i z - jkct],$$

$$(5)$$

where the wave-vector component normal to the plane of the film is given by

$$\alpha^i = {}^+[k^2\epsilon - (\mathbf{G}^i + \mathbf{k}_p)^2]^{1/2}. \qquad (6)$$

In the substrate (sub) we have only the transmitted beams:

$$\mathbf{H}_p^{\text{tra}} = \sum_i \mathbf{h}_{\text{tra}}^i \exp[j(\mathbf{G}^i + \mathbf{k}_p) \cdot \mathbf{r}_p - j\alpha_{\text{sub}}^i z - jkct]. \qquad (7)$$

The corresponding in-plane electric-field components can be found straightforwardly from Maxwell's equations, and for this we make a numerical Fourier expansion of

the function ϵ^{-1}.   Let the interfaces of the film be at $z = \pm L/2$, where L is the total film thickness.   We then have the following boundary conditions:

$$\sum_i (\mathbf{H}_p^{\text{inc},i} + \mathbf{H}_p^{\text{ref},i})|_{z=+L/2} = \sum_i \mathbf{H}_p^{\text{pc},i}|_{z=+L/2},$$

$$\sum_i (\mathbf{E}_p^{\text{inc},i} + \mathbf{E}_p^{\text{ref},i})|_{z=+L/2} = \sum_i \mathbf{E}_p^{\text{pc},i}|_{z=+L/2},$$

$$\sum_i \mathbf{H}_p^{\text{tra},i}|_{z=-L/2} = \sum_i \mathbf{H}_p^{\text{pc},i}|_{z=-L/2},$$

$$\sum_i \mathbf{E}_p^{\text{tra},i}|_{z=-L/2} = \sum_i \mathbf{E}_p^{\text{pc},i}|_{z=-L/2}.$$

$$(8)$$

We retain N reciprocal lattice vectors in all the Fourier expansions.   Matrix $\mathbf{M}$ in Eq. (3) will then have dimensions $2N \times 2N$, and so it will have $2N$ eigenvectors. Each of these $2N$ eigenvectors can have corresponding complex β values of either sign, giving a total of $4N$ Bloch modes, the amplitudes of which are unknown.   Also, there are $2N$ reflected beams with unknown amplitudes $\{h_{x,\text{ref}}^i, h_{y,\text{ref}}^i\}$ and similarly $2N$ transmitted beams.   The incident amplitudes are prespecified, and so we have a total of $8N$ unknowns.   Fortunately, the boundary conditions stated above impose $8N$ linearly independent constraints; so a unique solution exists for any given set of incident amplitudes.

3. CHARACTERISTICS OF VCSER's

We now analyze the case of a film of $\text{Al}_x\text{GaAs}_{1-x}$ (refractive index, 3.46; thickness, 240 nm) etched through with a triangular lattice of holes (radius, 56 nm; spacing, 500 nm) and placed on a substrate of oxidized $\text{Al}_y\text{GaAs}_{1-y}$ (index, 1.6), the cover being air.   The excitation wavelength is 980 nm, and the incident polarization state is TM. When the transmittance is plotted against $\mathbf{k}_p/k$ ($\mathbf{k}_p$ being the component of the incident wave vector parallel to the surface of the film), a whole sequence of extremely sharp resonances appears, superimposed on a slowly varying background (Fig. 2).   The sharp peaks and troughs in transmittance T are caused by excitation of high-Q-factor Bloch-wave resonances within the film.   The positions of these resonances are sensitive functions of the film parameters.

A. Comparison with Uniform Film
It is instructive to compare this behavior with that of a uniform film 240 nm thick with a refractive index of 3.46, placed on the same substrate and excited with TM-polarized 980-nm light.   As shown in Fig. 2, no Fabry–Perot resonances are apparent, although the slowly varying response closely follows the slowly varying background transmittance of the photonic crystal layer. Clearly the lattice of air holes has a very dramatic effect on the optical properties of the layer.

B. Loci of VCSER's in Reciprocal Space
The loci in $\mathbf{k}_p$ space of these high-Q VCSER's are plotted in Fig. 3.   In general, an arbitrarily polarized incident
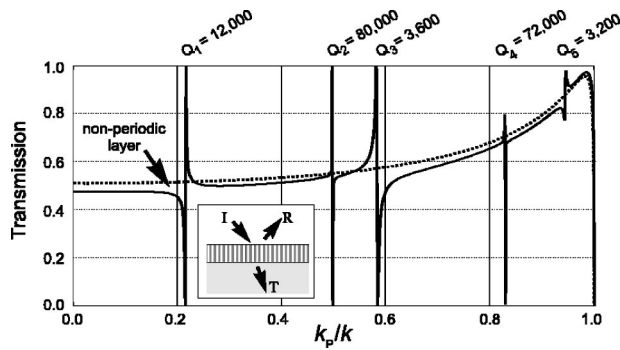
Fig. 2.   Transmittance of the modeled photonic crystal film (see inset for geometry) against $\mathbf{k}_p$, featuring three main VCSER's. For comparison the transmission of a layer of the same thickness, with the same refractive index as the dielectric but containing no holes, is also plotted.   The Q values of the resonances are noted on the plot.   The in-plane direction of incidence is $(\Gamma - J)$, and the incident polarization is TM.   These resonances correspond to the open circles in Fig. 3.
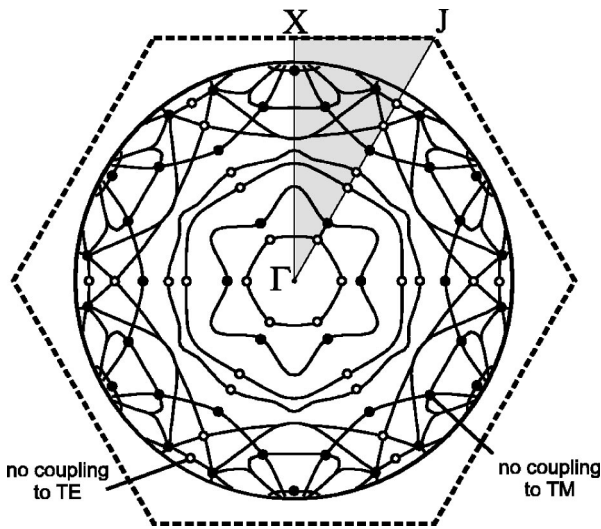

Fig. 3.   Calculated map of VCSER loci in $\mathbf{k}_p$ space.   Also shown are the isolated points at which the VCSER's cannot be excited with pure TM light (solid circles) or with pure TM light (open circles).   The hexagon is the boundary of the first Brillouin zone.

beam can excite a VCSER, but there are certain isolated points in the wave-vector diagram at which the VCSER's are uncoupled to incident light of a particular polarization state.   The small circles correspond to cases in which resonances are not excited by TE light and the disks to cases in which TM light is uncoupled from the resonances.   At these isolated points, light still penetrates the film—it simply does not excite high-Q resonances.

C.   Bloch Wave Spectrum of VCSER's
At any particular angle of incidence a whole set of propagating Bloch waves is excited.   In Fig. 4 the allowed values of $\beta(k_{px}, k_{py}, \omega)$ are plotted along the $\Gamma - J$ trajectory in the $\mathbf{k}_p$ plane.   The positions of the VCSER's in Fig. 2 are marked with dashed vertical lines, the dominant Bloch waves being indicated in each case.   It is remarkable that high-Q VCSER's can occur even where the photonic band structure of the film has no bandgaps or other

features.   This gives a lot of freedom in the choice of parameters when designing structures that support VCSER's.

D.   Field Microstructure of VCSER's
The extent of light confinement at VCSER's is shown by plotting the electromagnetic intensity in a vertical plane passing through the centers of a row of holes in the film.   Figure 5(a) is for VCSER 1 and Fig. 5(b) is for VCSER 2.   Note that for VCSER 1 the intensity is concentrated in the dielectric, while for VCSER 2 it is strongly concentrated in the holes.   The dominant Bloch waves in each case (Fig. 4) have low values of β when the VCSER is concentrated in the air and high values of β when the VCSER is concentrated in the dielectric.

E.   Line-Shape Characteristics
In Fig. 6 the time-averaged reflected, transmitted, and Bloch wave intensities are plotted against the in-plane wave vector for the first resonance in Fig. 2.   The Bloch-wave intensities are approximately Lorentzian in shape.   The reflected and the transmitted intensities behave rather differently, approximately following $\pm$ the derivative of a Lorentzian with an added constant.   This means that when a typical VCSER is excited externally (i.e., from outside the film), part of the incident power flux is
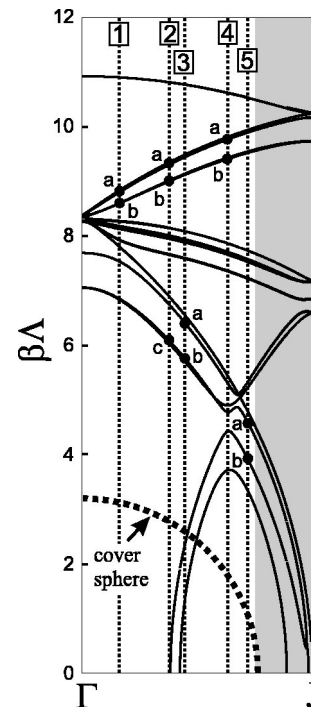

Fig. 4.   Corresponding band structure diagram β versus $\mathbf{k}_p$ along the $\Gamma - J$ direction for the case in Fig. 2.   Several propagating Bloch waves exist at every angle of incidence.   The positions of each of the five sharp VCSER's are indicated by the vertical dotted lines.   Only a small number (typically two to four) of these Bloch waves are significantly excited at each VCSER.   Their relative intensities (expressed as a percentage of the sum of the intensities of all the Bloch waves involved in each resonance) are as follows: VCSER 1, a = 65%, b = 33%; VCSER 2, a = 14%, b = 36%, c = 29%;   VCSER 3, a = 10%, b = 83%;   VCSER 4, a = 47%, b = 49%;   VCSER 5, a = 70%, b = 26%.
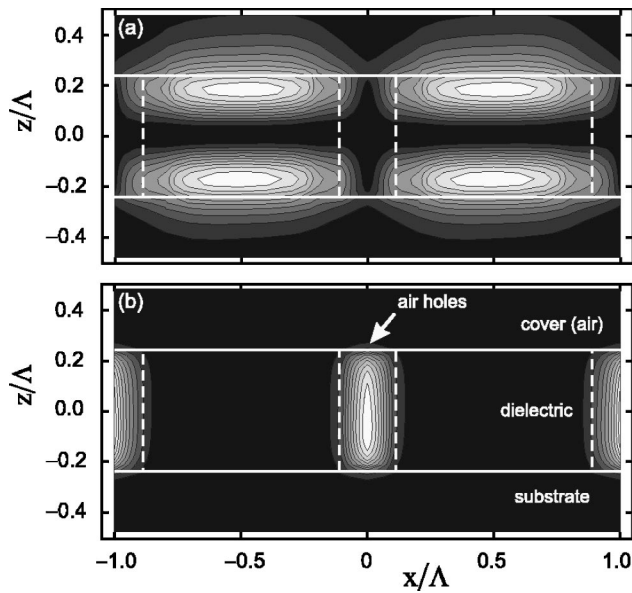
Fig. 5.   Electric-field intensity profiles of (a) VCSER 1 and (b) VCSER 2 in the plane $y = 0$.   The white dashed lines are the hole boundaries, and the white solid lines are the film interfaces.
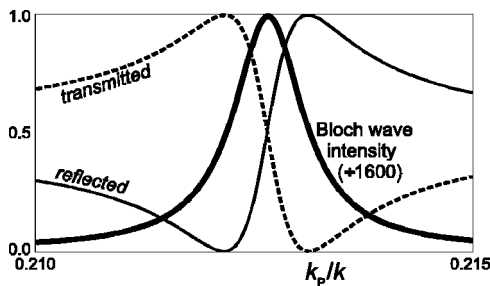

Fig. 6.   Transmittance (T) and reflectance ($R = 1 - T$) of the photonic crystal film against $\mathbf{k}_p$ in the locality of the first VCSER in Fig. 2, plotted together with the intensity of the strongest coresonant Bloch mode.

transmitted and part is reflected.   Only by slightly detuning from the center of the resonance can one obtain maximum transmission or maximum reflection (100% transmission and 100% reflection occur only in a few special cases).

F.   Toy Model
This unusual behavior can be explained as follows.   In a simple Fabry–Perot resonator there is only one internal wave, which bounces to and fro between the interfaces. In a photonic crystal film, however, several different Bloch waves are typically excited (see Fig. 7).   Therefore we modify the standard Fabry–Perot analysis to allow for several internal waves (coupled to each other at the substrate and cover interfaces), some with high transmission coefficients to the outside world and the others with low coefficients.   Imposing reciprocity, we obtain a system that behaves in a very similar way to our example photonic crystal film (see Appendix A).   The low-finesse resonances of a two-wave resonator provide background transmission and reflection, while its high-finesse resonances cause sharp features, and intercoupling between

them makes their corresponding transmission and reflection spectra non-Lorentzian.   An example is given in Fig. 8.

G.   Why Such High Q's?
Why is it that VCSER's in photonic crystal films have such high Q factors (as high as 80,000 in Fig. 2)? The answer lies in the high-reflection coefficients at the interfaces experienced by a few of the excited Bloch waves. These few Bloch waves give rise to resonances of very high finesse.   Their reflection coefficients are very high because their dominant plane waves have in-plane wave-vector components that lie beyond the boundaries of the substrate and cover cutoff circles.   This renders them unable to radiate significant power away from the film, while permitting nonzero coupling to the outside world through the very weak plane-wave whose in-plane wave vector lies inside the cover cutoff circle.
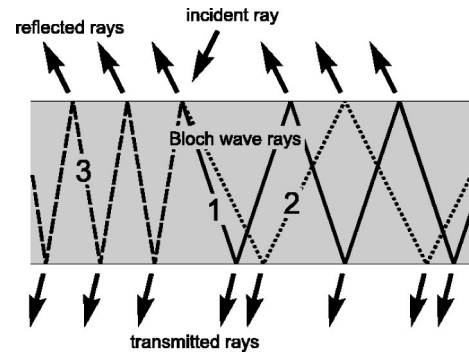

Fig. 7.   Photonic crystal film in which three Bloch waves are excited by the incidence of a single plane wave.   Note that the pitch is small enough to ensure that there are no diffracted rays—only transmitted and reflected ones.   The Bloch waves are in general both negatively and positively refracted.   By applying reciprocity to a toy model with two significant internal Bloch waves, it is possible to reproduce accurately the VCSER shapes in Fig. 2.   In a typical case only one Bloch wave is resonant (experiencing high reflection at the interfaces), the others providing low-finesse background resonances (experiencing only weak reflection at the interfaces).   The combination of these two yields the behavior in Fig. 2.
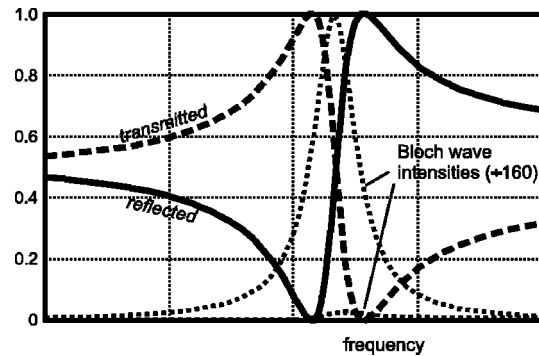

Fig. 8.   Solution generated by the toy model for two internal waves.   The parameter values used (chosen to satisfy reciprocity) are $\tau_{10} = 0.1$, $\tau_{20} = 0.9$, $\rho_{00} = -0.42$, $\rho_{11} = -0.98$, $\rho_{22} = 0.41$, and $\beta_1/\beta_2 = 1.5$.   The similarity with the behavior of a photonic crystal layer is striking.   More complex behavior results if more than two internal waves are included in the analysis.
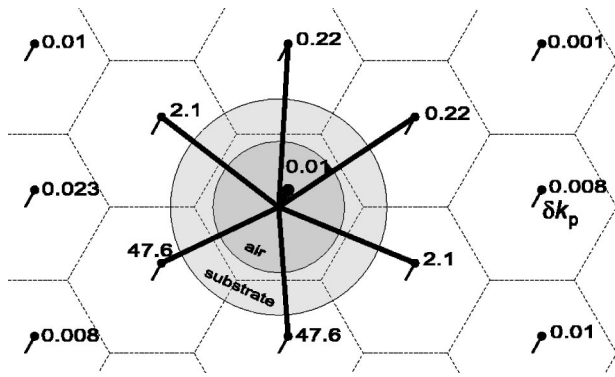
Fig. 9. Wave-vector diagram in the plane of the film. The shaded circles in the center indicate the zones where the substrate and cover regions are able to support traveling waves; beyond the largest of these circles the light is evanescent both in the air and in the substrate. The hexagonal regions are the tiled first Brillouin zones of the two-dimensional photonic crystal. The in-plane wave-vector components of one of the coresonant Bloch modes for VCSER 1 are indicated by small black dots; each is displaced from the center of its Brillouin zone by $\delta\mathbf{k}_p$. The intensities of each associated plane wave (expressed as a percentage of the sum of the intensities of all the plane waves) are indicated by the numbers alongside each dot. Note that almost 95% of the power is carried by two plane waves that are unable to radiate into the substrate or the cover. The only plane wave that can radiate into both substrate and cover carries only 0.01% of the power. This explains why such high Q factors are obtainable: The incident plane wave is only very weakly coupled to the Bloch wave resonances.

Figure 9 shows the intensities of the main plane-wave components of the most intense upward-traveling Bloch wave involved in VCSER 1. The horizontal and the vertical axes are the x and the y components of $\mathbf{k}_p$. The in-plane wave-vector components of one of the coresonant Bloch modes for VCSER 1 are indicated by the small black dots; each is displaced from the center of its Brillouin zone by $\delta\mathbf{k}_p$. Note that the wave vectors of the most intense plane-wave components of this Bloch-wave point in the opposite direction to the incident beam; in other words, this Bloch wave goes backward, and it goes backward because of another curious feature of Bloch-wave optics—negative refraction.[9]

The behavior can also be explained in terms of the resolution limit of light in air. If the Bloch wave microstructure is fine enough to be predominantly below the resolution limit of light in air, then it cannot readily radiate into air, giving rise to high-Q resonances. As pointed out in 1992,[10] Bloch waves can yield superresolution owing to the very high values of the wave vector that the higher-order plane-wave components possess.

4. DESIGN

The number and Q factors of the VCSER's can be controlled by altering the air-filling fraction, pitch, and film thickness. For example, a film of 15 nm thick (otherwise having the same parameters as in Fig. 2) supports only one resonance for TM-polarized light at 980 nm (Fig. 10). This resonance has $Q = 200,000$. In Fig. 11 the TM transmission characteristics of a film with a hole radius of 120 nm (other parameters as for Fig. 2) are plotted. A single low-finesse resonance appears with $Q = 120$.

Thus we see that it is possible to design structures with a wide range of different Q factors simply by varying the geometry of the film.

5. CONCLUSIONS

In summary, we have related the properties of a photonic crystal film under external illumination to its Bloch modes in a rigorous and intuitive way. Our calculation method allows one to develop the physical insight necessary to design more elaborate thin-film photonic crystal devices. The modes of a photonic crystal film are much more controllable than those of an unpatterned film. For suitable parameter values a photonic crystal film can act as a high-Q-factor optical resonator, the electric field being concentrated either in the holes or in the solid regions of the film. This would allow the selective enhancement of electromagnetic interactions with the film material or with gas or vapor in the holes. Photonic crystal VCSER's have important potential applications in vertical cavity surface-emitting lasers and gas/vapor sensing.
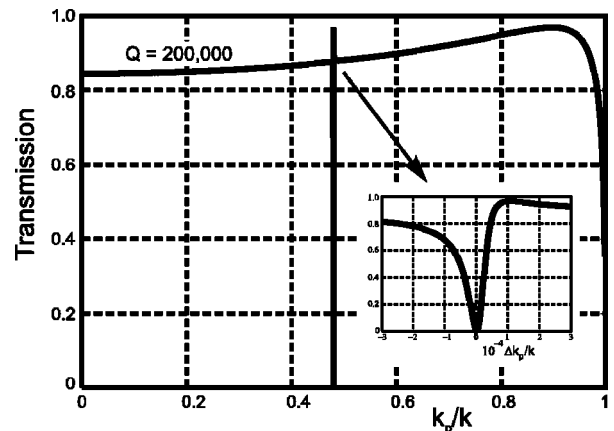

Fig. 10. Transmittance of a film 15 nm thick (and otherwise the same parameters as in Fig. 2), plotted versus $\mathbf{k}_p/k$ in the $\Gamma-J$ direction. It supports only one VCSER for TM-polarized light at 980 nm. This VCSER has $Q = 200,000$.
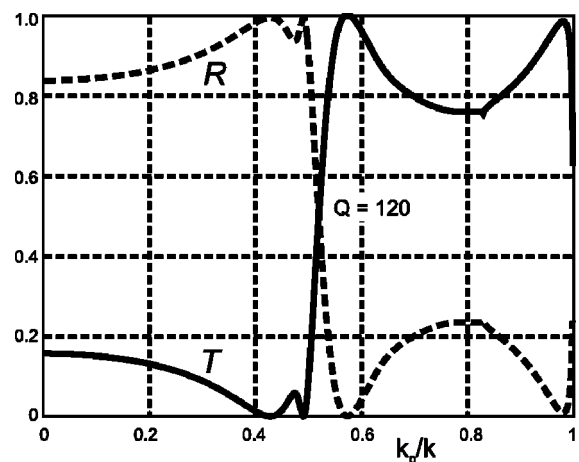

Fig. 11. TM transmission characteristics of a film with a hole radius of 120 nm, but otherwise the same parameters as in Fig. 2, plotted versus $\mathbf{k}_p/k$ in the $\Gamma-J$ direction. A single low-finesse VCSER appears with $Q = 120$.
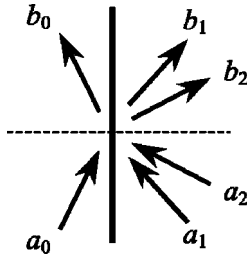
Fig. 12. Wave amplitudes in the single-interface transfer matrix for a structure in which two internal waves are present on one side of the interface. All three incident waves are coupled to each other at the interface as well as being reflected and refracted.

APPENDIX A

The scattering matrix for a lossless interface, with three incident waves (two internal and one external; see Fig. 12) can be written in the form

$$\begin{pmatrix} b_0 \\ b_1 \\ b_2 \end{pmatrix} = \mathbf{M}_T \begin{pmatrix} a_0 \\ a_1 \\ a_2 \end{pmatrix} = \begin{bmatrix} \rho_{00} & \tau_{01} & \tau_{02} \\ \tau_{01} & \rho_{11} & \rho_{12} \\ \tau_{02} & \rho_{12} & \rho_{22} \end{bmatrix} \begin{pmatrix} a_0 \\ a_1 \\ a_2 \end{pmatrix},$$

$$\mathbf{M}_T \mathbf{M}_T = \mathbf{I}. \tag{A1}$$

The second equation, which imposes reciprocity on the matrix coefficients, allows one to find algebraic expressions for the reflection and the transmission amplitudes in terms of τ_{01} and τ_{02}. It is then straightforward to treat a symmetrical Fabry–Pérot resonator with two internal waves. For unit incident amplitude from the external medium, the following are the transmitted and the reflected amplitudes:

$$T = \mathbf{QL}[\mathbf{I} - (\mathbf{NL})^2]^{-1}\mathbf{B}_0,$$

$$R = \rho_{00} + \mathbf{QLNL}[\mathbf{I} - (\mathbf{NL})^2]^{-1}\mathbf{B}_0, \tag{A2}$$

where

$$\mathbf{Q} = (\tau_{01}, \tau_{01}), \qquad \mathbf{N} = \begin{bmatrix} \rho_{11} & \rho_{12} \\ \rho_{12} & \rho_{22} \end{bmatrix}, \tag{A3}$$

$$\mathbf{L} = \begin{bmatrix} \exp(-j\beta_1 L) & 0 \\ 0 & \exp(-j\beta_2 L) \end{bmatrix}, \qquad \mathbf{B}_0 = \begin{pmatrix} \tau_{10} \\ \tau_{20} \end{pmatrix}. \tag{A4}$$

The wave-vector components (normal to the layer) of the two internal waves are β_1 and β_2, and the layer thickness is L.

*Permanent address, Departament d'Òptica, Universitat de València, Spain; e-mail, enrique.silvestre@uv.es.

†Address correspondence to P. St. J. Russell at the address on the title page or by e-mail, p.s.j.russell@bath.ac.uk.

REFERENCES

1. O. Painter, R. K. Lee, A. Scherer, A. Yariv, J. D. O'Brien, P. D. Dapkus, and I. Kim, "Two-dimensional photonic bandgap defect mode laser," Science **284**, 1819–1821 (1999).
2. H. Kosaka, T. Kawashima, A. Tomita, M. Notomi, T. Tamamura, T. Sato, and S. Kawakami, "Photonic crystals for micro lightwave circuits using wavelength-dependent angular beam steering," Appl. Phys. Lett. **74**, 1370–1372 (1999).
3. P. St. J. Russell, "Novel thick-grating beam-squeezing device in Ta_2O_5 corrugated planar waveguide," Electron. Lett. **20**, 72–73 (1984).
4. R. Zengerle, "Light propagation in single and doubly periodic planar waveguides," J. Mod. Opt. **34**, 1589–1617 (1987).
5. P. St. J. Russell, T. A. Birks, and F. D. Lloyd-Lucas, "Photonic Bloch waves and photonic band gaps," in *Confined Electrons and Photons*, E. Burstein and C. Weisbuch, eds. (Plenum, New York, 1995), pp. 585.
6. P. St. J. Russell, D. M. Atkin, T. A. Birks, and P. J. Roberts, "Bound modes of two-dimensional photonic crystal waveguides," in *Quantum Optics in Wavelength Scale Structures*, J. G. Rarity and C. Weisbuch, eds. (Kluwer Academic, Dordrecht, The Netherlands, 1996).
7. D. M. Atkin, P. St. J. Russell, T. A. Birks, and P. J. Roberts, "Photonic band structure of guided Bloch modes in high index films fully etched through with periodic microstructure," J. Mod. Opt. **43**, 1035–1053 (1996).
8. V. N. Astratov, I. S. Culshaw, R. M. Stevenson, D. M. Whittaker, M. S. Skolnick, T. F. Krauss, and R. M. De La Rue, "Resonant coupling of near-infrared radiation in photonic band structure waveguides," J. Lightwave Technol. **17**, 2050–2057 (1999).
9. P. St. J. Russell and T. A. Birks, "Bloch wave optics in photonic crystals: physics and applications," in *Photonic Band Gap Materials*, C. M. Soukoulis ed., (Kluwer Academic, Dordrecht, The Netherlands, 1996), pp. 71–91.
10. P. St. J. Russell, "Photonic band-gaps," Phys. World **5**, 37–42 (1992).